

Upper Field Strength Limit of Fast Radio Bursts

YU ZHANG AND HUI-CHUN WU^{1,*}

¹*Institute for Fusion Theory and Simulation and Department of Physics, Zhejiang University, Hangzhou 310027, China*

ABSTRACT

Fast radio bursts (FRBs) are cosmological radio transients with unclear generation mechanism. Known characteristics such as their luminosity, duration, spectrum and repetition rate, etc. suggest that FRBs are powerful coherent radio signals at GHz frequencies, but the status of FRBs near source remain unknown. As an extreme astronomical event, FRBs should be accompanied by energy-comparable or even more powerful x/ γ -ray counterparts. Here, particle-in-cell simulations of ultra-strong GHz radio pulse interaction with GeV photons show that at $\gtrsim 3 \times 10^{12}$ V/cm field-strengths, quantum cascade can generate dense pair plasmas, which greatly dampen the radio pulse. Thus, in the presence of GeV photons in the source region, GHz radio pulses stronger than 3×10^{12} V/cm cannot escape. This result indicates an upper field-strength limit of FRB at the source.

Keywords: Radio bursts(1339); Radio transient sources (2008); Plasma astrophysics (1261)

1. INTRODUCTION

Since first discovered in 2007 (Lorimer et al. 2007), fast radio bursts (FRBs) have been recognized as real astronomical events and gain much research interest (Katz 2018; Platts et al. 2019; Zhang 2020). Although event reports and theoretical models of FRBs have exploded over the past decade, the origin of FRBs remains unclear. Due to large dispersion measures with hundreds or even thousands of cm^{-3}pc , these radio transients have cosmological origins (Xu & Han 2015), which has been confirmed by several events with located host galaxies (Thornton et al. 2013; Petroff et al. 2016). Therefore FRBs can be served as novel probes for interstellar and intergalactic matters (Prochaska et al. 2019; Macquart et al. 2020).

Assuming an isotropic emission, the luminosity of FRBs ranges from 10^{38} to 10^{45} erg/s (Thornton et al. 2013; Zhang 2018), many orders of magnitude more powerful than radio pulsars. Meanwhile, the ultrahigh brightness temperature $\sim 10^{35}$ K (Katz 2018; Zhang 2020) indicates that FRB radiations must be coherent. The millisecond duration implies that the source is limited to hundreds of kilometers in size, which points to compact objects in universe, such as white dwarfs, neutron stars, or black holes. The observed FRB200428 (Bochenek et al. 2020; CHIME/FRB et al. 2020; Lin et al. 2020) in the Milky Way associated with a hard X-ray burst from magnetar SGR1935+2154, suggest magnetars can generate FRBs.

Many models of FRBs (Katz 2018; Platts et al. 2019; Zhang 2020) have been proposed. Possible FRB sources are located in- or out-side of the magnetospheres of neutron stars. In the magnetosphere, the radiation mechanisms include plasma maser emissions from relativistic plasmas or plasma instabilities (Lyubarsky 2020), and curvature radiation of charged bunches (Kumar et al. 2017; Katz 2014; Yang et al. 2020; Lu & Kumar 2018). Outside of the magnetosphere, relativistic shocks driven by outflows from neutron stars may also induce FRBs (Lyubarsky 2014; Waxman 2017; Metzger et al. 2019; Beloborodov 2020). Although the emission region of the FRBs in neutron stars is still being debated, most theoretical models show that FRBs are accompanied by energy comparable or even more powerful counterparts in x and γ rays bands of keV-to-TeV (Chen et al. 2020). The observed x-rays from FRB200428 are four orders of magnitude more energetic than the radio emission.

FRBs have been detected in the range of 0.3-8 GHz (Zhang 2020), with a bandwidth of hundreds of MHz limited by the detection band of radio telescopes. The coherent GHz radiation implies an emitter in the sub-meter scale. In the immediate vicinity of the emitters, FRB corresponds to an extremely strong microwave. Research on this extreme microwave is rare (Wu 2016). In this paper we simulate the interaction between ultra-strong GHz radio waves and GeV gamma photons. It is found that at field-strength of 3×10^{12} V/cm, dense pair plasmas are produced by quantum cascades that significantly dampen the radio pulses. This process should occur in the FRB emission region and constrains the radiation intensity near the emitters.

* huichunwu@zju.edu.cn

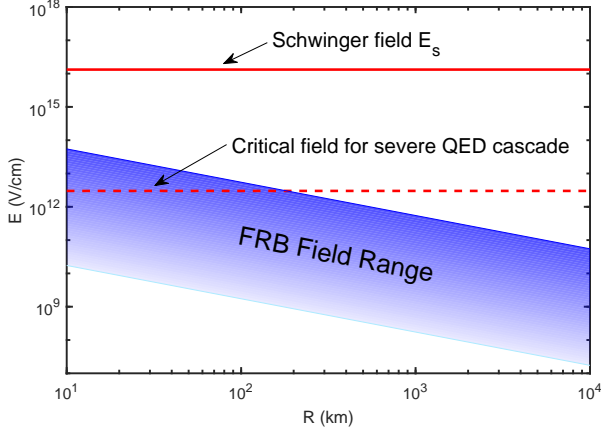


Figure 1. Estimated FRB field strength E as a function of the distance R from sources.

2. INTERACTION OF STRONG RADIO WAVE AND HIGH-ENERGY PARTICLES

2.1. Estimation of the FRB field strength near the source

The FRB energy can be expressed as $W = d\Omega R^2 cT \varepsilon_0 E^2$, where $d\Omega$ is the solid angle of the FRB emission cone, E is the field amplitude at a distance R from the source, $T \approx 1\text{ms}$ is the duration, c is the light speed, and ε_0 is the vacuum permittivity. For isotropic emission ($d\Omega = 4\pi$), the energy range is estimated to be $W_i = 10^{35} \sim 10^{42}\text{erg}$, so that the field strength E can be obtained from

$$W_i = 4\pi R^2 cT \varepsilon_0 E^2. \quad (1)$$

It is stressed that here R only refers to a distance from the FRB emitters, which may be located in the inner or outer magnetospheres of neutron stars.

The blue region in Figure 1 shows the possible E range of FRB as a function of R . The field strength range is $1.7 \times 10^9 \sim 5.4 \times 10^{12}\text{V/cm}$ for $R = 100$ km. The solid line marks the Schwinger field $E_s = 1.32 \times 10^{16}\text{V/cm}$. The dashed line is the critical field strength $3 \times 10^{12}\text{V/cm}$ predicted by our simulations, where high-energy photons can trigger strong quantum cascades and radiation damping. For a point source, E in Equation (1) will diverge when $R \rightarrow 0$. The actual emission zone should consist of many emitters and have a total emission surface of area S . The emission energy has $W = ScT \varepsilon_0 E^2$, similar to Equation (1). For $S = 10^5\text{km}^2$, $E = 1.95 \times 10^9 \sim 6.14 \times 10^{12}\text{V/cm}$.

2.2. 1D PIC-QED code

To investigate the interaction between ultrastrong FRBs and gamma photons, we use the one-dimensional particle-in-cell simulation code JPIC1d-QED, where avalanche quantum-electrodynamics (QED) production of positron-electron pairs through the Breit-Wheeler process and nonlinear inverse Compton scattering (Elk-

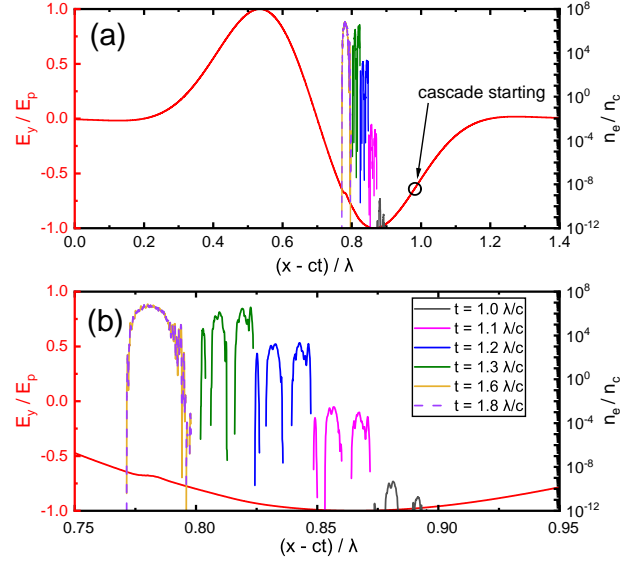


Figure 2. (a) Distribution of electron density n_e (the positron density is effectively the same) in the comoving frame with the electric field E_y . (b) An enlargement of the electron densities n_e in (a).

ina et al. 2011; Erber 1966; Kirk et al. 2009) are included in the existing code JPIC1d (Wu 2011). Production of positron-electron pairs and photons are determined by a Monte-Carlo algorithm with quantum generation rates (Elkina et al. 2011; Wang et al. 2017; Nerush et al. 2011). A particle-merging scheme is used to deal with the rapidly increased particles in the avalanche. To suppress numerical noises typically encountered in PIC-QED simulations, we adopt a five-point particle interpolation for the positrons/electrons. The code has been benchmarked for single-electron quantum cascades in a static magnetic field (Elkina et al. 2011; Angelou & Vankov 1999) and reproduced the results of ultraintense laser QED breakdowns triggered by a single electron (Nerush et al. 2011).

The Breit-Wheeler process generates electron-positron pairs by annihilation of gamma photons in intense electromagnetic fields. Inverse Compton scattering in turn generates gamma photons by the FRB field accelerated relativistic electrons and positrons. Both these effects are measured by (SI units):

$$\chi \simeq \frac{\gamma}{E_s} \sqrt{(\mathbf{E} + \mathbf{v} \times \mathbf{B})^2 - (\mathbf{v} \cdot \mathbf{E})^2 / c^2} \quad (2)$$

where γ is the Lorentz factors of electrons/positrons and photons; \mathbf{v} is the particle speed; and \mathbf{E} and \mathbf{B} are the electric and magnetic fields, respectively. For photons, $\gamma = \epsilon/mc^2$ and $|\mathbf{v}| = c$, ϵ is the photon energy, and m is the electron rest mass. Obvious QED cascades can occur for $\chi \simeq 0.1$, and massive production of pairs and photons occurs when $\chi \rightarrow 1$.

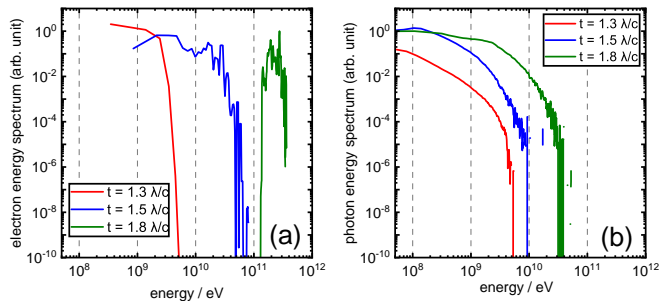


Figure 3. Electron energy spectra (a) and photon energy spectra (b) at $t = 1.3\lambda/c$, $1.5\lambda/c$ and $1.8\lambda/c$. Positrons have the almost same energy spectrum as electrons.

2.3. Nanosecond-duration radio pulse and GeV gamma photon

A hundreds-MHz bandwidth implies a coherent time of a few nanoseconds, thus the millisecond FRBs are expected to contain many coherent nanosecond subpulses. We now consider the interaction between such nanosecond subpulse and gamma photons and attempt to find the critical field strength for substantial quantum cascades within the subcycle of radio waves. Dense-pair plasmas generated in the subcycle can dampen a great portion of the entire multiple-cycle pulse (Nerush et al. 2011). Since FRBs are highly polarized, we assume the bipolar waveform $E_y = E_0 \exp(-t^2/\tau^2) \sin(\omega_0 t)$ in our simulations, where $\omega_0/2\pi = 1\text{GHz}$ is the central frequency, and $\tau = 0.3\lambda/c$ for wavelength $\lambda \sim 30\text{cm}$. The radio pulse propagates along the x axis and the peak field strength is $E_p = 0.636E_0$ due to the carrier-envelope phase effect.

Although TeV radiations are also predicted to associate with FRB events, here we focus on the GeV-level triggering particles, which are not a rigorous requirement for extreme environments in neutron stars (Becker 2009). Quantum cascade is sensitive to the interaction angle between fields and particles. From Equation (2), one obtains

$$\chi \simeq \frac{\gamma}{E_s} (E_y - v_x B_z) = \frac{\gamma E_y}{E_s} (1 - \frac{v}{c} \cos \theta) \quad (3)$$

where θ is the angle between the particle velocity v and the x axis. The QED effects are negligible for $\theta = 0$ and most pronounced for head-on collision with $\theta = 180^\circ$. For $\gamma = 2000$ and $\theta = 180^\circ$, the field strength for quantum cascades at $\chi = 0.1$ is $E = 3.3 \times 10^{11}\text{V/cm}$.

It is difficult for the GeV charged particles to trigger quantum cascade in the FRB fields, since the electrons and positrons will be decelerated in the longitudinal direction by the ultrastrong ponderomotive force of FRB fields, then get reflected and copropagate (at $\theta \sim 0$) with the radio waves. Such reflection occurs for the incident particle with energy less than $\gamma_{rf} \sim a_0/4$ (Wu et al. 2011), where $a_0 = eE/mc\omega_0$. For 1 GHz radio waves with $E = 3.3 \times 10^{11}\text{V/cm}$, one has $a_0 = 3.1 \times 10^6$

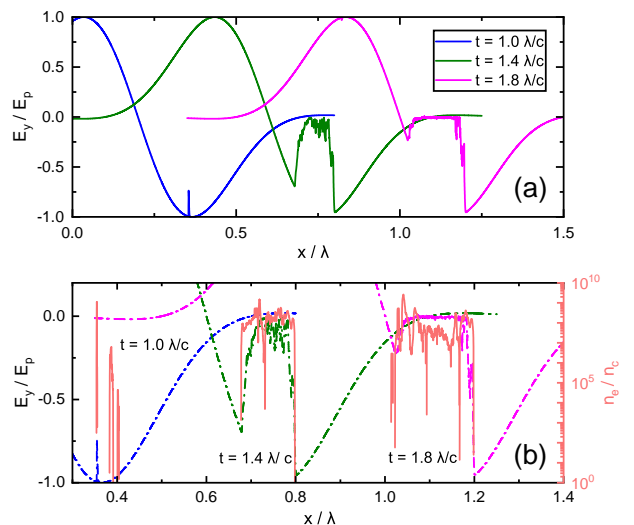


Figure 4. (a) Distribution of E_y at $t = 1\lambda/c$, $1.4\lambda/c$, and $1.8\lambda/c$. (b) Enlargement of a region in (a) and n_e . The dashed and solid curves represent E_y and n_e , respectively.

and $\gamma_{rf} \approx 7.8 \times 10^5$, i.e., 0.4 TeV. However, as to be shown below, if the pair particles can emit energetic gamma photons, quantum cascade will be possible since the gamma photons can freely penetrate into the strong FRB fields and annihilate into electron-positron pairs.

3. RESULTS

The first simulation is conducted for $E_p = 2.68 \times 10^{12}\text{V/cm}$, which corresponds to $a_0 = eE_p/mc\omega_0 \simeq 2.5 \times 10^7$ and magnetic field of $E_p/c \simeq 0.89 \times 10^{10}$ Gauss. The simulation box is 2λ in length with a spatio/temporal resolution of 10000 grids per wavelength/cycle. Ten 1 GeV photons simultaneously incident to the FRB pulse with $\theta = 120^\circ$.

Figure 2 shows photon-triggered pair plasma sparks in the comoving frame of the radio pulse. Obvious QED cascades occur at $E_y \approx 0.7E_{p0}$, where annihilation of incident photons generates hundreds of $\chi \sim 0.1$ pair particles, which are in turn violently accelerated by the intense FRB fields to ultra-relativistic energies and emit high-energy photons. The latter are further annihilated into electron-positron pairs by the FRB fields. As shown in Figure 2, three distinct plasma clumps appear, they grow and finally merge into a plasma sheet within ~ 1 ns. The plasma density increases exponentially before the clump merges and saturates at $t = 1.6\lambda/c$ with the peak density of $7.2 \times 10^6 n_c$. Here, $n_c \simeq 1 \times 10^{13} (\text{cm}/\lambda)^2 \text{cm}^{-3} = 1.11 \times 10^{10} \text{cm}^{-3}$ is the critical density for 1 GHz waves. After $t = 1.6\lambda/c$, the pair plasma sheet comoves with the field, and hence quantum cascades cease. For an ultra-relativistic field, the plasma density for screening the field is $\sim a_0 n_c$. The plasma sheet has a density lower than $a_0 n_c = 2.5 \times 10^7 n_c$ and its thickness is 0.01λ . Thus it causes only a small distortion on the FRB field.

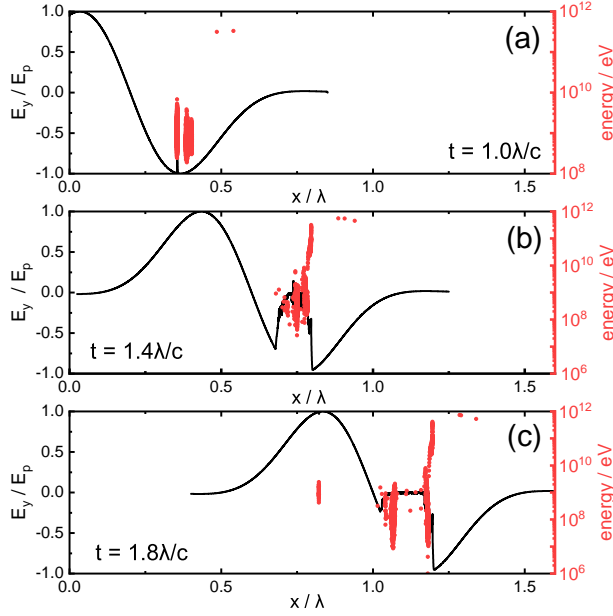


Figure 5. Electron energy distribution superposed with the field at (a) $t = 1\lambda/c$, (b) $t = 1.4\lambda/c$ and (c) $t = 1.8\lambda/c$.

Figure 3 shows the electrons and photons energy spectra. During the active cascades at $t \sim 1.3\lambda/c$, the particles and photons are synergetic with each other and have almost the same maximum energy. However, due to the wave field acceleration, the charged particle energy are always more concentrated than the photon energy. After the saturation at $t \sim 1.5\lambda/c$, the charged particles are free from radiation damping, and their energy quickly overtake that of the photons. They are more monoenergetic than before, and have an average energy ~ 0.2 TeV at $t = 1.8\lambda/c$.

We increase the peak wave field to $E_p = 3 \times 10^{12}$ V/cm with $a_0 = 2.8 \times 10^7$. Figure 4 shows the electric field E_y and pair plasma density n_e . Due to the generated pair plasmas, partial field screening starts at $t \sim 1\lambda/c$. Then the plasma density dramatically increases and exceeds the relativistic critical density $a_0 n_c \sim 2.8 \times 10^7 n_c$. The field screening then becomes complete in the plasma with $n_e > a_0 n_c$, and the pair plasma expands towards the frontside and further grows to the backside. Figure 5 shows the electron energies distribution. At the front of the plasma, electrons/positrons are further accelerated along the x axis to higher energies. According to Equation (3) the QED effects becomes weak and pairs are no longer produced. On the backside, the oscillating charged particles on the vacuum-plasma boundary continues to collide with the right-going field and produce new pairs. However, Fig. 5(b) and (c) show that due to the continuous radiation damping, the energy of these particles are suppressed, as compared with that of the accelerated particles on the right front. In Figure 5(c), one can see that a plasma spark appears downstream in the second half cycle. It is triggered by the emitted pho-

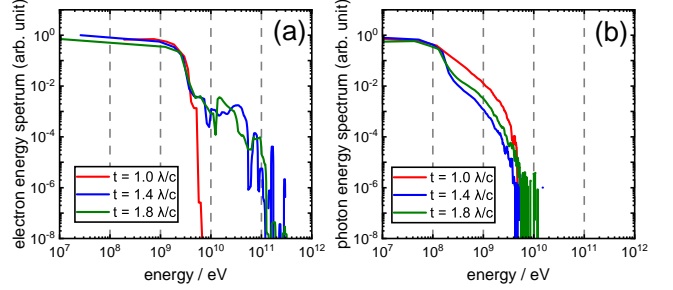


Figure 6. Electron energy spectra (a) and photon energy spectra (b) at $t = 1\lambda/c$, $1.4\lambda/c$ and $1.8\lambda/c$.

tons from the QED-active backside of the pair plasma region. Such sparks could dampen the FRB field in the more extended space.

Energy spectra of electrons and photons are given in Figure 6. During the active quantum cascades at $t = 1\lambda/c$, charged particles and photons have similar spectra as that in figure 3. After the complete field screening, the high-energy part of the spectra at $t = 1.4\lambda/c$ and $1.8\lambda/c$ in Figure 6(a) comes from the field accelerated particles at the plasma front. Depletion of GeV photons at $1\lambda/c < t < 1.4\lambda/c$ can be attributed to photon annihilation and production of pair plasmas.

Gamma photons above 1 GeV are observed to more easily cause the field depletion. We also carried out the simulations for charged particles in GeV-TeV range and found that tens GeV are required to trigger significant radiation damping. In 3D space, pair plasmas will fill the main radio-field volume, as demonstrated in multi-dimensional PIC simulation of ultraintense laser breakdown triggered by a single electron in vacuum (Nerush et al. 2011). On the other hand, here we have only tens photons interacting with the FRB. Existing models invoke photons with comparable high energy (GeV-TeV) co-existing with the FRBs. The results here indicate that such high-energy photons will fully deplete the FRB.

For FRBs propagating cross the neutron star magnetic field B_{NS} , incoherent scattering by magnetospheric plasmas could be significant and gamma rays produced in this process would trigger severe cascades in the FRB (Beloborodov 2021). When radio waves propagate along the background magnetic field B_{NS} , gamma-photon annihilation due to B_{NS} is negligible due to the vanishing term $\mathbf{v} \times \mathbf{B}_{NS} = 0$ in Eq. (2). Therefore, our results are more applicable for FRBs escaping from the polar regions of neutron stars.

As an extremely efficient radio burst, the plasma/beam emitter must be able to coexist with its self-field and radiation field, and will not induce severe field breakdown within both emitter and FRB bodies. According to our results, this requires that the plasma density in or nearby the emitter should be lower than the level of $a_0 n_c$ for less field screening, and the

plasma/beam driver could mainly propagate along the radiation direction for negligible pair cascades. The driver can produce high-energy gamma rays along its momentum direction. By Compton backscattering from background plasmas, these gamma rays could turn back to scatter the FRB field as studied here.

4. CONCLUSION

We have investigated radiation dampings of FRBs triggered by high-energy photons in GeV. At the field amplitude of 3.0×10^{12} V/cm, dense pair plasmas are generated within sub-cycle of these radio transients.

The plasma generation and radiation absorption lead to breakdown of FRBs fields. This energy depletion can critically limit the field-strength of FRBs around their emitters. Similar QED effects can also be expected during other stages of FRB propagation. Our work also implies that QED effects (Philippov et al. 2020; Katz 2017) could be indispensable near the FRB emitter.

This work was supported by the Strategic Priority Research Program of Chinese Academy of Sciences (Grant No.XDA17040503). We thank W. M. Wang and M. Y. Yu for helpful discussions.

REFERENCES

- Anguelov, V., & Vankov, H. 1999, *Journal of Physics G: Nuclear and Particle Physics*, 25, 1755
- Becker, W. 2009, *Neutron Stars and Pulsars*, 1st edn., Vol. 357 (Berlin, Heidelberg: Springer-Verlag)
- Beloborodov, A. M. 2020, *The Astrophysical Journal*, 896, 142
- . 2021, *The Astrophysical Journal Letters*, 922, L7
- Bochenek, C. D., Ravi, V., Belov, K. V., et al. 2020, *Nature*, 587, 59
- Chen, G., Ravi, V., & Lu, W. 2020, *The Astrophysical Journal*, 897, 146
- CHIME/FRB, C., et al. 2020, *Nature*, 587, 54
- Elkina, N., Fedotov, A., Kostyukov, I. Y., et al. 2011, *Physical Review Special Topics-Accelerators and Beams*, 14, 054401
- Erber, T. 1966, *Reviews of Modern Physics*, 38, 626
- Katz, J. 2014, *Physical Review D*, 89, 103009
- . 2017, *Monthly Notices of the Royal Astronomical Society: Letters*, 469, L39
- . 2018, *Progress in Particle and Nuclear Physics*, 103, 1
- Kirk, J. G., Bell, A., & Arka, I. 2009, *Plasma Physics and Controlled Fusion*, 51, 085008
- Kumar, P., Lu, W., & Bhattacharya, M. 2017, *Monthly Notices of the Royal Astronomical Society*, 468, 2726
- Lin, L., Zhang, C., Wang, P., et al. 2020, *Nature*, 587, 63
- Lorimer, D. R., Bailes, M., McLaughlin, M. A., Narkevic, D. J., & Crawford, F. 2007, *Science*, 318, 777
- Lu, W., & Kumar, P. 2018, *Monthly Notices of the Royal Astronomical Society*, 477, 2470
- Lyubarsky, Y. 2014, *Monthly Notices of the Royal Astronomical Society: Letters*, 442, L9
- . 2020, *The Astrophysical Journal*, 897, 1
- Macquart, J.-P., Prochaska, J., McQuinn, M., et al. 2020, *Nature*, 581, 391
- Metzger, B. D., Margalit, B., & Sironi, L. 2019, *Monthly Notices of the Royal Astronomical Society*, 485, 4091
- Nerush, E., Kostyukov, I. Y., Fedotov, A., et al. 2011, *Physical review letters*, 106, 035001
- Petroff, E., Barr, E., Jameson, A., et al. 2016, arXiv preprint arXiv: 1601.03547
- Philippov, A., Timokhin, A., & Spitkovsky, A. 2020, *Physical review letters*, 124, 245101
- Platts, E., Weltman, A., Walters, A., et al. 2019, *Physics Reports*, 821, 1
- Prochaska, J. X., Macquart, J.-P., McQuinn, M., et al. 2019, *Science*, 366, 231
- Thornton, D. e. a., Stappers, B., Bailes, M., et al. 2013, *Science*, 341, 53
- Wang, W.-M., Gibbon, P., Sheng, Z.-M., Li, Y.-T., & Zhang, J. 2017, *Physical Review E*, 96, 013201
- Waxman, E. 2017, *The Astrophysical Journal*, 842, 34
- Wu, H.-C. 2011, arXiv preprint arXiv:1104.3163
- . 2016, *Scientific reports*, 6, 1
- Wu, H.-C., Meyer-ter-Vehn, J., Hegelich, B., Fernández, J., et al. 2011, *Physical Review Special Topics-Accelerators and Beams*, 14, 070702
- Xu, J., & Han, J. 2015, *Research in Astronomy and Astrophysics*, 15, 1629
- Yang, Y.-P., Zhu, J.-P., Zhang, B., & Wu, X.-F. 2020, *The Astrophysical Journal Letters*, 901, L13
- Zhang, B. 2018, *The Astrophysical Journal Letters*, 867, L21
- . 2020, *Nature*, 587, 45